Amino Acids (2012) 43:389–396
DOI 10.1007/s00726-011-1093-x

ORIGINAL ARTICLE

# Solution structure of a novel α-conotoxin with a distinctive loop spacing pattern

**Bingbing Zhang · Feijuan Huang · Weihong Du**

Received: 27 May 2011 / Accepted: 19 September 2011 / Published online: 4 October 2011


**Abstract** α-Pharmacological conotoxins are among the most selective ligands of nicotinic acetylcholine receptors with typical cysteine frameworks. They are characterized by the intercysteine loop and classified into various subfamilies, such as α3/5 and α4/7 conotoxins. A novel α-conotoxin, Pu14a (D**C**PPHPVPGMHK**C**V**C**LKT**C**), with a distinct loop spacing pattern between cysteines was reported recently. Pu14a belongs to the Cys framework 14 (–C–C–C–C) family containing four proline residues in the loop 1 region. Similar to another framework 14 conotoxin Lt14a (M**C**PPL**C**KPS**C**TN**C**-$NH_2$), Pu14a has C1–C3/C2–C4 disulfide linkage, and can inhibit some subtypes of nicotinic acetylcholine receptors. In this study, the solution structure of Pu14a was investigated using $^1$H nuclear magnetic resonance spectroscopy to understand the structure-activity relationship of this conotoxin. 20 converged structures of this conopeptide, with RMSD value of 0.77 Å, were obtained based on distance constraints, dihedral angles and disulfide bond constraints. The three-dimensional structure of Pu14a showed remarkable difference from typical α-conotoxins because of a large intercysteine loop between C2 and C13, as well as a $3_{10}$-helix near the C-terminal. Furthermore, four proline residues in Pu14a adopted the *trans* conformation that may correlate with the large loop configuration and the biological activity of this conopeptide. The distinct structural characteristics of Pu14a will be very useful for studying the structure-activity relationship of α-conotoxins.

**Keywords** α-Conotoxin · Pu14a · Solution structure · Proline

## Introduction

Cone snail venoms are a rich source of peptides that target various neuroreceptors, ion channels, and transporters (Terlau and Olivera 2004; Oliveral et al. 2008). A number of studies on conotoxins have shown that these peptides, which are mostly small (typically 10–40 amino acids) and disulfide-rich, can serve as valuable probes for neurophysiological studies (Olivera and Cruz 2001; Janes 2005; Olivera et al. 1985) and potential tools for drug discovery (McIntosh et al. 2000; Craik and Adams 2007). Some classification schemes are used to describe aspects of conotoxins: "gene superfamily," "cysteine framework," and "pharmacological family" schemes (Kaas et al. 2010).

Based on the targeted receptor and the type of interaction with the receptor, conopeptides are classified into 11 pharmacological families, such as the α-, ω-, δ-, μ-, κ-pharmacological family, and 21 cysteine frameworks by various cysteine residue patterns in the sequence (Kaas et al. 2008). Conopeptides that target the nicotinic acetylcholine receptor (nAChR) are designated to the most populated family, the α-pharmacological family (Janes 2005). Defining the subfamily, according to the number of residues between two consecutive cysteines, is a very useful classification in investigating the structure-function relationship between α-conotoxins and different nAChR subtypes. For example, α-conotoxins MI from *Conus magus* (McIntosh et al. 1982) and GI from *C. geographus* (Gray et al. 1981) belong to the subfamily of α3/5; these species show a high binding affinity toward the α/δ subtype of nAChR. PnIA from *C. pennaceus* (Luo et al. 1999) and

**Electronic supplementary material** The online version of this article (doi:10.1007/s00726-011-1093-x) contains supplementary material, which is available to authorized users.

B. Zhang · F. Huang · W. Du (✉)
Department of Chemistry, Renmin University of China, Beijing 100872, China
e-mail: whdu@chem.ruc.edu.cn

AnIA from *C. anemone* (Loughnan et al. 2004) belong to the subfamily of α4/7; these species are selective for α3β2 or α3β4-containing receptors. α-Conotoxin ImI, the first neuronally active toxin and identified as α4/3, block the neuromuscular α7 subtype of nAChR and is potent toward the α9 subtype of nAChR (McIntosh et al. 1994). These studies show that the loop spacing pattern has a remarkable influence on the biological functions of conopeptides.

Different nAChR subtypes are implicated in learning, pain sensation, and disease states, including Parkinson's disease and nicotine addiction. Studies indicate that the nAChR-binding site is composed of a hydrophobic region containing conserved aromatic residues from both α and β subunits (Jensen et al. 2005). The different concentration-responses of F119 on wild-type α3β2 nAChR and mutation receptors of T59K, V111I, and F119Q reveal that F119 has relatively considerable effects on the binding interaction between ligands and nAChR subunits (Luo et al. 2010). In addition, hydrophobic residues, such as Leu and Val, occupying special positions in conopeptide sequences are significant in enhancing the affinity of a conopeptide to nAChR (Nicke et al. 2003; Lopez-Vera1 et al. 2007). The mutation of K7A in Lt14a exhibits higher activity than in native Lt14a, indicating that charged residues may play a vital role in target recognition (Peng et al. 2006; Sun et al. 2010). As for the residue in the C-terminal of neuromuscular-selective a-conotoxins, the side chain with positive charge gives rise to greater potency than a neutral one in that position (Janes 2005).

Pu14a, a novel conotoxin with two disulfide bonds and multiple proline residues, was identified from *C. pulicarius* (Peng et al. 2010). This conotoxin belongs to the 14th cysteine framework (C–C–C–C) similar to Lt14a and shares high sequence identity with ts14a. Moreover, Pu14a has the same disulfide linkage (C1–C3, C2–C4) with that of numerous α-conotoxins, such as PnIA and EI (Park et al. 2001) (Table 1). Recent study reported that 1uM of Pu14a strongly inhibited the mouse neuromuscular α1β1γδ subtype of nAChR, blocking ~82% of the Ach-evoked current. At the same toxin concentration, the Ach-evoked current was blocked by ~55% in α6α3β2 subtype of the rat neuronal nAChR, then rapidly dissociated from the receptor. While 10 μM Pu14a exhibited ~51% block effect on α3β2 subtype of the rat neuronal nAChR. However, this toxin had no inhibitory effect on potassium channels in mouse superior cervical ganglion neurons (Peng et al. 2010) Furthermore, Pu14a has a distinct loop spacing pattern with $C(X_{10})C(X_1)C(X_3)C$, which is not observed in α-conotoxins. However, the structural feature of Pu14a remains unexplored. Among the identified framework 14 conopeptides, Lt14a can also inhibit the neuronal-type nAChR. Despite the differences in sequences and loop patterns between Pu14a and Lt14a, these conopeptides may have similar structural characteristics between them to target nAChR. In this study, we reported the solution structure of Pu14a using two-dimensional (2D) $^1$H nuclear magnetic resonance (NMR) method. Moreover, we re-determined the structure of Lt14a because its coordinates were not released. A comparison between Pu14a and Lt14a showed that Pu14a has a unique loop size and secondary structure elements different from those of Lt14a. The results of this study provide valuable information on the structure-activity relationship of α-conotoxins.

## Materials and methods

### Peptide synthesis

A sample of Pu14a was synthesized and identified as reported previously (Peng et al. 2010). To obtain enough NMR samples, the peptides, including Pu14a and Lt14a, were further chemically synthesized by SBS Co. Ltd. (Beijing, China). Furthermore, the peptides were identified by high performance liquid chromatography and mass spectrometry with more than 95% certainty.

### NMR experiments

The NMR samples were prepared by dissolving Pu14a and Lt14a in 500 μL of either 99.99% $D_2O$ (Cambridge Isotope Lab, MA, USA) or 9:1 (v/v) $H_2O/D_2O$ with 0.01% trifluoroacetic acid (St. Louis, USA) at pH 3.0. The final peptide concentration was approximately 4.0 mM.

**Table 1** Several conotoxins and their pharmacological activities

| name | Primary structure | Disulfide Connectivity | Specificity | Target | Reference |
|---|---|---|---|---|---|
| Pu14a | -----D**C**PPHPVPGMHK**C**V----------**C**LKT----**C** | C1-C3, C2-C4 | C(X10)C(X1)C(X3)C | α1β1γδ, α6α3β2, α3β2 | Peng et al. 2010 and this work |
| Lt14a | -----M**C**PPL-------**C**KPS---------**C**TN-----**C*** | C1-C3, C2-C4 | C(X3)C(X3)C(X2)C | n-AChR | Peng et al. 2006; Sun et al. 2010 and this work |
| LtIA | -----G**C**----------**C**ARAA--------**C**AGIHQEL**C*** | C1-C3, C2-C4 | α4/7 | α3β2 | Pi et al. 2006 |
| PnIA | -----G**C**----------**C**SLPP--------**C**AANNPDY**C*** | C1-C3, C2-C4 | α4/7 | α3β2, α3β4 | Luo et al. 1999 |
| ImI | -----G**C**----------**C**DPR---------**C**AWR----**C*** | C1-C3, C2-C4 | α4/3 | α7 | Gehrmann et al. 1999 and Armishaw et al. 2006 |
| EI | ---RDO**C**----------**C**YHPT--------**C**NMSNPQI**C*** | C1-C3, C2-C4 | α4/7 | α1δ | Park et al. 2001 |
| ts14a | ----DG**C**PPHPVPGMHP**C**M----------**C**TNT----**C** | C1-C3, C2-C4 | C(X10)C(X1)C(X3)C | - | Peng et al. 2010 |
| Pl14a | FPRPRI**C**NLA-------**C**RAGIGHKYPF--**C**H------**C**R* | C1-C3, C2-C4 | C(X3)C(X10)C(X1)C | Kv1.6, α3β4, α1β1εδ | Imperial et al. 2006 |
| Vil14a | -GGLGR**C**IYN-------**C**MNSGGGLSFIQ-**C**KTM----**C**Y | C1-C4, C2-C3 | C(X3)C(X11)C(X3)C | $K^+$ channels | Möller et al. 2005 |

NMR measurements were performed using standard pulse sequences and phase cycling on Bruker Avance 400 and 600 MHz NMR spectrometer (Germany) at 293 K. Proton DQF-COSY, NOESY and TOCSY spectra were acquired with the transmitter set at 4.70 ppm and a spectral window of 6,000 Hz. All 2D NMR spectra were acquired in a phase-sensitive mode using time-proportional phase incrementation for quadrature detection in the t1 dimension. Presaturation during the relaxation delay period was used to suppress the solvent resonance. NOESY spectra were acquired with mixing time of 350 ms. TOCSY spectra were acquired with a spin lock of 120 ms. The sample lyophilized from the $H_2O$ solution was redissolved in $D_2O$ to identify the slow exchange of backbone amide protons. One-dimensional (1D) $^1H$ spectra were measured after 5 min and every 10 min thereafter up to 5 h. All chemical shifts were referenced to the methyl resonance of 4,4-dimethyl-4-silapentane-1-sulfonic acid (DSS) used as internal standard. The spectra were processed using Bruker Topspin 2.1 and analyzed by Sparky 3.0. Final matrix sizes were usually 4,096 × 2,048 real points.

The structural information on Lt14a was reported in a previous study (Sun et al. 2010). Nevertheless, we re-determined the solution structure of Lt14a to obtain more detailed information. The acquired NOESY spectrum for Lt14a was undesirable because the small molecular weight of this peptide resulted in numerous missing NOE cross-peaks. The ROESY experiment was performed for this peptide to obtain a sufficient number of NOE constraints and calculate the solution structure. The ROESY spin lock was set at 200 ms.

### Distance restraints and structure calculations

A set of distance constraints was derived from the NOESY spectrum of Pu14a and the ROESY spectrum of Lt14a. Distance constraints, representing unambiguously assigned dipolar couplings, were used for structural calculations by Cyana 2.1. Dihedral angle restraints were determined based on the $^3J_{HN\text{-}H\alpha}$ coupling constants derived from the DQF-COSY spectral analysis. The $\varphi$ angle constraints for some residues were set to $-120 \pm 40°$ for $^3J_{HN\text{-}H\alpha} > 8.0$ Hz (C2, V7, G9, H11, and C15 for Pu14a; C2, C6, C10, and C13 for Lt14a) and $-65 \pm 25°$ for $^3J_{HN\text{-}H\alpha} < 5.5$ Hz (none was found in the NMR spectra). Backbone dihedral constraints were not applied for $^3J_{HN\text{-}H\alpha}$ values between 5.5 and 8.0 Hz. Distance constraints of the hydrogen bond were added as target values of 0.18–0.22 nm for the HN(i)—O(j) bond and 0.28–0.32 nm for the HN(i)—O(j) bond. The C-terminal amidation was produced in the Cyana library as a new residue to calculate the structures of Lt14a because C-terminal amidation has a significant influence on the folding tendency and the biological activity of a conotoxin (Kang et al. 2005). 100 random structures were generated to fit covalent and spatial requirements according to the primary sequence. The outcomes of Pu14a and Lt14a were a set of 20 lowest energy structures. The outcomes were used for structural quality analysis by MOLMOL software (Koradi et al. 1996).

## Results

### Sequence-specific resonance assignments

Two-dimensional NMR spectroscopy was used to examine the 3D structure of conotoxin Pu14a in aqueous solution at pH 3.0. The sequence-specific resonance assignments were achieved using the traditional visual analysis method (Wuthrich 1986). The spin systems of most amino acids were resolved by the TOCSY and DQF-COSY spectra. Figure 1 shows a representative portion of the Pu14a TOCSY spectrum in $H_2O$. Thirteen expected cross peaks between the amide proton and $H_\alpha$ were observed. Other spin systems were found in the fingerprint region of the TOCSY spectrum, and their assignments were verified in the fingerprint region of the DQF-COSY spectrum. The sequential assignments of amino acids in the primary sequence started with the unique residues G9, L16, and T18. A NOESY walk identified the residues from P4 to G9 toward the N-terminus and the residues from G9 to C19 toward the C-terminus. Owing to the missing amide proton of D1 and C2, the first three residues at the N-terminal were finally assigned based on the three spin systems, the cross peak between the $H_\alpha$ of C2 and $H_\beta$ of C15, and the cross peak between the $H_\alpha$ of C2 and $H_\delta$ of P3. The amide proton of D1 disappeared in the $H_2O$ spectrum possibly because of its special position at the N-terminal and fast exchange in water.

Twelve of the 13 spin systems were found in the fingerprint region of the 120 ms Lt14a TOCSY spectrum. The

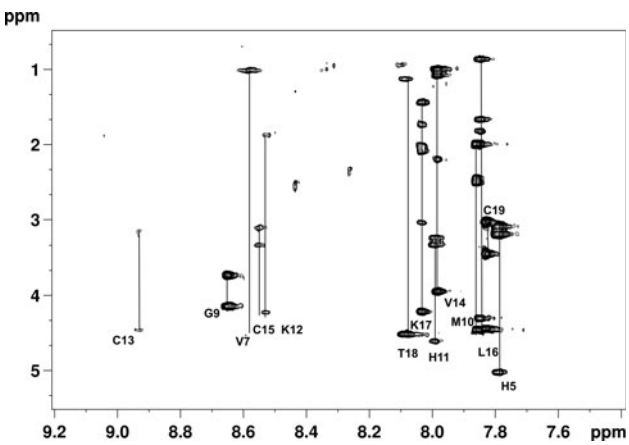


**Fig. 1** HN(*x*-axis)-aliphatic(*y*-axis) region of the H-H TOCSY spectrum for Pu14a at 298 K, pH 3.0

sequential assignments of amino acids in the primary sequence started with the unique residues L5, K7, and T11. Hence, NOE sequential walks along the N-terminus were identified. P8 was assigned by its spin system and the NOE from its $\delta$-proton to the $\alpha$-proton of G7. The methionine residue at position 1 was finally assigned according to the NOEs from the $\alpha$- and $\beta$-protons of Met1 to the amide proton of C2. NOE connectivities from T11 to the C-terminus were also identified. In addition, a minor component of this synthesized conotoxin with a proportion of 15% was observed (see supporting material Fig. 1S).

The NOESY data acquired for the two conopeptides showed a number of NOEs, suggesting that the structures of the peptides were sufficiently restrained for distance-geometry calculation. All Pu14a chemical shifts are listed in Table 2. The final chemical shifts of Lt14a (data not shown) were basically similar to the chemical shifts reported recently (Sun et al. 2010).

## Structure calculation and evaluation

The constraints for determining Pu14a structure were obtained from a survey of NMR data. A total of 179 distance constraints were used and the NOE root mean square violation was no more than 0.2 Å. The major NOE connectivity is shown in Fig. 2. Moreover, five $\varphi$ angle constraints and two disulfide bond constraints from C2 to C15 and C13 to C19 for Pu14a were input for the molecular modeling protocol of the Cyana algorithm. Although the

**Table 2** Proton resonance assignments (ppm) for Pu14a

| Residue | HN | $\alpha$ | $\beta$ | Other |
|---|---|---|---|---|
| Asp1 | | 4.27 | 2.68, 2.81 | |
| Cys2 | | 5.00 | 3.20, 2.91 | |
| Pro3 | | 4.73 | 2.34 | $\gamma$: 1.93, 2.00; $\delta$: 3.84, 3.67 |
| Pro4 | | 4.27 | 2.20 | $\gamma$: 1.69; $\delta$: 3.73 |
| His5 | 7.79 | 5.02 | 3.09, 3.19 | $\delta$: 7.24; $\varepsilon$: 8.46 |
| Pro6 | | 4.42 | 2.21,1.90 | $\gamma$: 1.96, 2.03; $\delta$: 3.60, 3.73 |
| Val7 | 8.56 | 4.52 | 2.14 | $\gamma$: 1.00 |
| Pro8 | | 4.34 | 2.34,1.91 | $\gamma$: 2.00, 2.12; $\delta$: 3.72,3.93 |
| Gly9 | 8.65 | 3.73, 4.14 | | |
| Met10 | 7.86 | 4.45 | 2.00 | $\gamma$: 2.45, 2.51; $\varepsilon$: 2.19 |
| His11 | 7.99 | 4.61 | 3.23, 3.33 | $\delta$: 7.24; $\varepsilon$: 8.29 |
| Lys12 | 8.54 | 4.22 | 1.87 | $\gamma$: 1.46 $\delta$: 1.70; $\varepsilon$: 3.00 |
| Cys13 | 8.91 | 4.46 | 3.14, 3.22 | |
| Val14 | 7.99 | 3.94 | 2.20 | $\gamma$: 1.00, 1.07 |
| Cys15 | 8.56 | 4.70 | 3.13, 3.33 | |
| Leu16 | 7.85 | 4.30 | 1.82 | $\gamma$: 1.66; $\delta$: 0.86 |
| Lys17 | 8.04 | 4.21 | 2.08, 2.01 | $\gamma$: 1.44; $\delta$: 1.72; $\varepsilon$: 3.04 |
| Thr18 | 8.09 | 4.52 | 4.46 | $\gamma$: 1.12 |
| Cys19 | 7.83 | 4.44 | 3.02, 3.45 | |

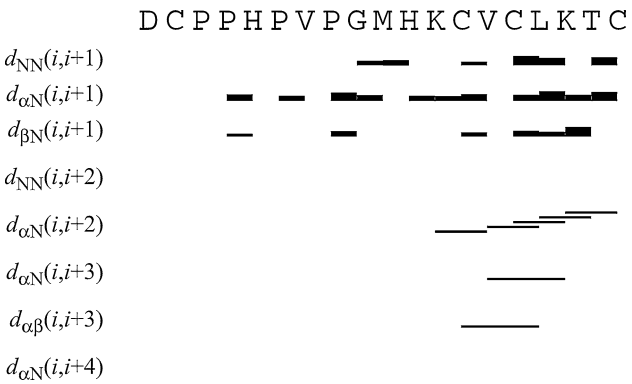


**Fig. 2** Summary of the sequential NOE connectivities involving the NH, $H_\alpha$, and $H_\beta$ protons measured at 293 K and mixing time of 350 ms for Pu14a

H-bond constraints were not found by H–D exchange experiments, existing constraints were enough for the structural calculation of such a small-sized peptide. As for Lt14a, 134 distance constraints, 4 dihedral restraints, 2 H-bond restraints from H–D exchange experiments, and 2 disulfide bonds from C2 to C10 and C6 to C13 were used to build up the structures. The structure of Lt14a was calculated using the data from a major conformer, and a 15% minor component was not considered at this stage.

First, we computed 20 solution structures to evaluate the folding of the peptidic chain using medium-distance constraints that have more than two bond intervals $|i-j| > 2$. Subsequently, all distance constraints and dihedral restraints were used. Then, H-bond constraints were introduced into the calculations. The simulated annealing calculations were started with 100 random structures. Finally, the ensemble of the 20 best resulting models with the lowest residual target function and the minimum root mean square deviation (RMSD) were selected. The resulting conformers contained no significant violation of any constraint. The Ramachandran plots were chosen to represent the 3D folding of Pu14a and Lt14a in a solution at pH 3.0. A summary of statistics for the converged structures evaluated in terms of structural parameters are listed in Table 3. The NMR constraints and obtained coordinates files were submitted to the BMRB database with ID code 21015 for Pu14a and 21014 for Lt14a.

## Solution structure of Pu14a

An overlay of the backbone atoms for the 20 structures of Pu14a is shown in Fig. 3a. The overall average backbone RMSD reported for the final 20 structures of Pu14a was $0.77 \pm 0.26$ Å. The N-terminal of these structures poorly converged because of the few constraints at this region. The refined structure of conotoxin Pu14a contains a larger loop between C2 and C13, rather than a $\omega$-type twist in the

**Table 3** Structural statistics for 20 structures of Pu14a and Lt14a

| Assigned NOE cross peaks | Pu14a | Lt14a |
|---|---|---|
| Intra-residue | 112 | 68 |
| Sequential | 49 | 21 |
| Medium range | 14 | 6 |
| Long range | 4 | 1 |
| H bond constraints | 0 | 2 |
| Dihedral constraints | 5 | 4 |
| RMSD to mean coordinates | | |
| Mean global backbone atoms RMSD | 0.77 ± 0.26 | 0.46 ± 0.18 |
| Mean global heavy atoms RMSD | 1.11 ± 0.24 | 0.69 ± 0.24 |
| Rachandran statistics from PROCHECK_NMR | | |
| Most favored regions (%) | 53.3 | 36.4 |
| Additional allowed regions (%) | 44.6 | 54.3 |
| Generously allowed regions (%) | 0 | 9.3 |
| Disallowed regions (%) | 2.1 | 0.0 |

center of typical α-conotoxins, such as PnIA and EI. Although three intercysteine loops of Pu14a could be described by the sequence, only one real loop existed between C2 and C13. The real loop corresponded to the intercysteine loop 1 containing 10 residues. Interestingly, in the so-called intercysteine loop 2 (with one residue V14) and loop 3 (with 3 residues L16, K17 and T18) regions, the secondary structural elements of $3_{10}$-helix and turns were obtained (Fig. 4a). Inspection of NOE constraints revealed that the NOE connections for V14$H_{\alpha}$-K17HN ($i$–$i$ + 3), V14$H_{\alpha}$-L16HN ($i$–$i$ + 2) and C13$H_{\alpha}$-L16$H_{\beta}$ ($i$–$i$ + 3) were observed in Pu14a. The folding of residues C13 to L16 tended to form a $3_{10}$-helix, though no H-bond constraints were added in the calculation process. On the other hand, the side chains of most residues, except P3 and V14, were oriented outside (Fig. 3b).

## Comparison of Pu14a with other α-conotoxins

The structural feature of Pu14a was quite different from those of typical α-conotoxins, such as PnIA. A comparison

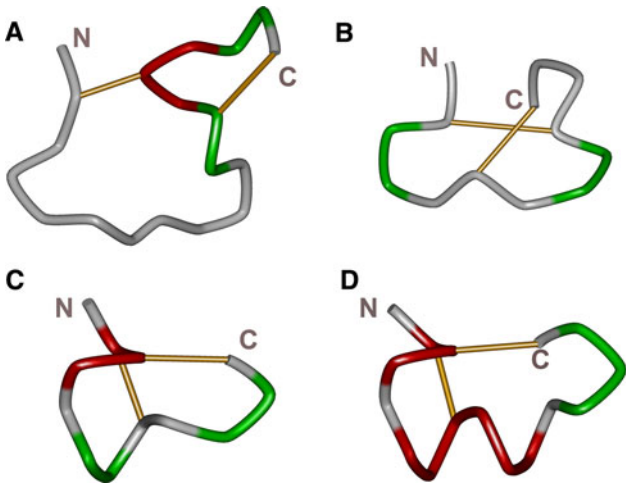


**Fig. 4** Mean structures of conotoxins illustrated in tube mode. **a** Pu14a, **b** Lt14a, **c** ImI (PDB ID: 1NCL) and **d** PnIA (PDB ID: 1PEN). The disulfide bond is shown in *stick*. Underlying secondary structure features were analyzed by MOLMOL. The images are generated by ViewerLite software

of the backbone structures of Pu14a, Lt14a, ImI, and PnIA is shown in Fig. 4. The illustrated structure of Lt14a was based on our determination in the present study. The average backbone RMSD reported for the final 20 structures of Lt14a was 0.46 ± 0.18 Å with 2 H-bond constraints and 0.32 ± 0.19 Å without H-bond constraints, besides other constraints used. It indicated that the structures of Lt14a were well resolved. Except for the N-terminal residue M1, the refined structure of Lt14a contained two turns similar to that reported in a previous study (Sun et al. 2010). Moreover, the loop region found in Lt14a was smaller than that in Pu14a.

As shown in Fig. 4, the backbone structure of Pu14a was distinct from that of PnIA, although they both inhibited the $\alpha 3\beta 2$ subtype of nAChR. Interestingly, the backbone structure of Lt14a exhibited remarkable resemblance to that of PnIA despite their distinct secondary structure elements. Albeit in the same cysteine framework of 14, both Pu14a and Lt14a are the ligands of different subtypes of nAChR, and their conformational profiles are dissimilar.

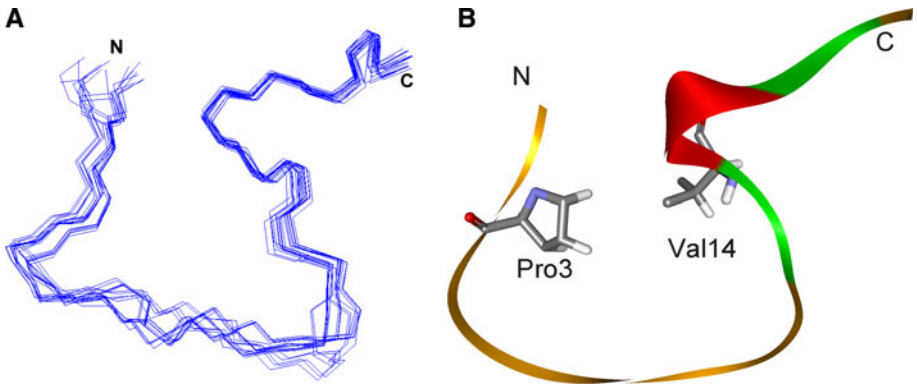


**Fig. 3** **a** Overlay of the backbone atoms for the 20 converged structures of conotoxin Pu14a. The N-terminal D1 is poorly resolved. **b** Inward side chain orientation of P3 and V14 in Pu14a

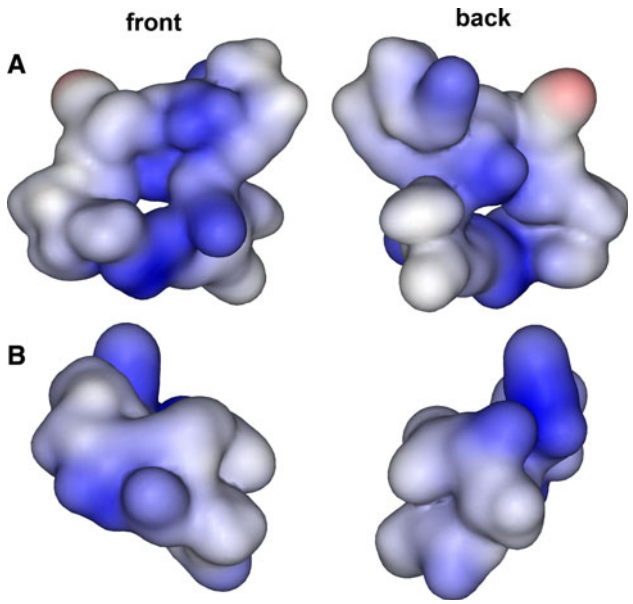


**Fig. 5** Surface representations of **a** Pu14a and **b** Lt14a are shown in front and back views. The ViewerLite software was used to produce these images

Pu14a has a relatively larger volume than Lt14a (see supporting material Fig. 2S). Furthermore, the loop of Pu14a was large enough to form a pore in the loop center, which can be displayed by the structural surfaces from the front and back views (Fig. 5).

## Discussion

### Distinct loop configuration of Pu14a

The present study describes the solution structure of a novel α-conotoxin Pu14a and compares its structure with that of another framework 14 conotoxin (Lt14a) and other α-conotoxins. α-Conotoxins, the largest pharmacological family in conotoxins, are extensively investigated. Most α-conotoxins are classified into different subfamilies as previously mentioned. Nevertheless, the loop spacing pattern of Pu14a is unique from that of other α-conotoxins. The loop pattern is $C(X_{10})C(X_1)C(X_3)C$ for Pu14a, whereas it is $C(X_3)C(X_3)C(X_2)C$ for Lt14a. Hence, the distinct loop spacing pattern possibly results in various backbone foldings and their corresponding effects on the biological functions of α-conotoxins. In addition, without a typical *ω*-type twist in the loop center, Pu14a also inhibits $\alpha 3\beta 2$-containing receptors such as PnIA. The relatively large loop 1 that existed in Pu14a was determined based on all of the constraints from the NMR spectra; moreover, the refined structure was credible because long-range distance constraints were used (see supporting material Table 1S). This result indicates that Pu14a may have a rather flexible conformation in solution, and it may be transformed when targeting nAChR.

### Tran X-P peptide bonds in Pu14a

Four proline residues, namely, P3, P4, P6, and P8, were found in the Pu14a sequence without hydroxylation, the popular posttranslational modification in conotoxins. By contrast, Lt14a has three proline residues at positions 3, 4, and 8. Observations of the NOE crosspeaks from $C2H_\alpha$-$P3H_\delta$, $P3H_\alpha$-$P4H_\delta$, $H5H_\alpha$-$P6H_\delta$ and $V7H_\alpha$-$P8H_\delta$ in the NOESY spectrum of Pu14a (Fig. 6) indicate that the X-P prolyl bonds were all in *trans* conformation in Pu14a. As for Lt14a, only those crosspeaks from $P4H_\alpha$-L5HN, $P4H_\delta$-L5HN, and $K7H_\alpha$-$P8H_\delta$ were observed in the ROESY spectrum. Considering the 15% minor component, either P3 or P4 was possibly in the *cis* conformation with its frontal residue.

Owing to the higher intrinsic energy difference between the *cis* and *trans* prolyl bond conformations, the *cis* isomer occurs rarely in polypeptides (Exarchos et al. 2009). A survey shows that 5.2% of X-P prolyl bonds (where X is any of the 20 amide acids and P represents proline) are in *cis* conformation, and only 0.03% of the X-nonP (where nonP denotes any other amino acid except proline) peptide bonds are in *cis* conformation (Weiss et al. 1998). The distinct occurrence for the *cis* and *trans* conformations is inferred to rely on the type of the secondary structure (Pahlke et al. 2005). Although both Pu14a and Lt14a have multiple proline residues with a special "-Cys-Pro-Pro-" sequential segment, the possible *cis* X-P prolyl bond appeared only in Lt14a, which may have been induced by their distinct secondary elements. Hence, we may hypothesize that all *trans* X-P prolyl bonds result in the unique loop configuration of Pu14a.

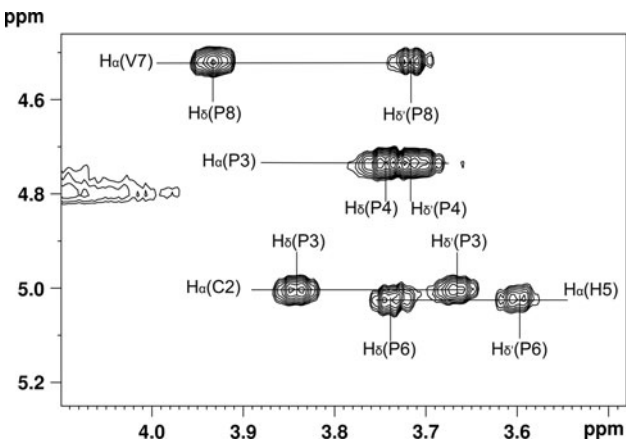


**Fig. 6** The NOE connectivities between the proline $H_\delta$ and the $H_\alpha$ of its frontal residues in Pu14a

## Structure-activity relationship of Pu14a

The structure of Pu14a is characterized by a large loop and a distinct $3_{10}$-helix. Pu14a can inhibit the mouse neuromuscular $\alpha1\beta1\gamma\delta$ subtype, the rat neuronal $\alpha6\alpha3\beta2$ and $\alpha3\beta2$ subtypes of nAChR. Interestingly, Pl14a, another framework 14 conotoxin with the structural feature of an α-helix and two $3_{10}$-helices, can inhibit the Kv1.6, neuronal $\alpha3\beta4$, and neuromuscular $\alpha1\beta1\varepsilon\delta$ subtypes of nAChR (Imperial et al. 2006). The $3_{10}$-helix is also observed in one of the most studied α-conotoxin, ImI, which exhibits full bioactivity on the α7 subtype of nAChR (Gehrmann et al. 1999). Pu14a, Lt14a, Pl14a, and ImI have the same disulfide linkages with C1-C3 and C2-C4 connectivities; nevertheless, the differences among the aforementioned conopeptides in terms of loop pattern and secondary structure elements reflect the relationship between their structures and bioactivities. The side chains of most residues in Pu14a, except P3 and V14, were oriented outside (Fig. 3b). However, all of the side chains in Lt14a were generally oriented outside. The inside orientation of nonpolar residues, including P3 and V14 in Pu14a, may improve the hydrophobic interaction between ligands and nAChR.

Recently, Luo's work elucidated an energetically favorable hydrophobic interaction between Lt1a-L15 and $\beta2$-F119 (Luo et al. 2010). Due to the block effect on $\alpha3\beta2$ for Pu14a, L16 was proposed to contribute to the energy minimization of the interaction and further stabilize the conformation of Pu14a-$\alpha3\beta2$. Based on Pu14a sequence, K17, a positively charged residue in the C-terminal region of α-conotoxin, gave rise to greater neuromuscular-selectivity than a neutral residue, as reported by Janes (Janes 2005).

Another framework 14 conopeptide, vil14a, has a Lys/Tyr dyad separated by approximately 6 Å, which is a conserved structural feature in K channel blockers (Möller et al. 2005). The pl14a sequence shows contiguous Lys/Tyr dyad. The Lys/X motif of pl14a is also distinct from that of vil14a. A Lys/X motif has a significant effect on the formation of H-bond between conotoxins and their targets. The great difference between Pu14a and vil14a in terms of their bioactivities may be related to their sequences, secondary structures, and Lys/X motifs.

In summary, the solution structure of Pu14a is distinct from other α-conotoxins because of its special loop spacing pattern. Compared with Lt14a, Pu14a has a larger volume and an additional proline residue that correlates with various secondary structural elements and X-P bond conformations. Pu14a conformation reflects the structural diversity and flexibility in α-conotoxins. These preliminary studies will help to understand the structure and activity relationships among different kinds of α-conotoxins. The distinctive loop spacing pattern and proline-rich sequence will be very beneficial for chemical modification of conotoxins to improve their stability and bioactivity, further for the design and development of potential peptide drugs.

**Acknowledgments** We thank Prof. Chunguang Wang and Prof. Chengwu Chi from Tongji University for supplying the sample of Pu14a friendly. This work was supported by the National Basic Research Program (No. 2011CB808503), and the Fundamental Research Funds for the Central Universities and the Research Funds of Renmin University of China (No. 10XNJ011).

**Conflict of interest** None.

## References

Armishaw CJ, Daly NL, Nevin ST, Adams DJ, Craik DJ, Alewood PF (2006) α-Selenoconotoxins, a new class of potent $\alpha_7$ neuronal nicotinic receptor antagonists. J Biol Chem 281:14136–14143

Craik DJ, Adams DJ (2007) Chemical modification of conotoxins to improve stability and activity. ACS Chem Biol 2:457–468

Exarchos KP, Exarchos TP, Papaloukas C, Troganis AN, Fotiadis DI (2009) Detection of discriminative sequence patterns in the neighborhood of proline *cis* peptide bonds and their functional annotation. BMC Bioinformatics 10:113

Gehrmann J, Daly NL, Alewood PF, Craik DJ (1999) Solution structure of α-Conotoxin ImI by $^1$H nuclearmagnetic resonance. J Med Chem 42:2364–2372

Gray WR, Luque A, Olivera BM, Barrett J, Cruz LJ (1981) Peptide toxins from *Conus geographus* venom. J Biol Chem 256: 4734–4740

Hu SH, Gehrman J, Guddat LW, Alewood PF, Craik DJ, Martin JL (1996) The 1.1 Å crystal structure of the neuronal acetylcholine receptor antagonist, α-conotoxin PnIA from *Conus pennaceus*. Structure 4:417–423

Imperial JS, Bansal PS, Alewood PF, Daly NL, Craik DJ, Sporning A, Terlau H, López-Vera E, Bandyopadhyay PK, Olivera BM (2006) A novel conotoxin inhibitor of Kv1.6 channel and nAChR subtypes defines a new superfamily of conotoxins. Biochemistry 45:331–8340

Janes RW (2005) α-Conotoxins as selective probes for nicotinic acetylcholine receptor subclasses. Curr Opin Pharmacol 5:280–292

Jensen AA, Frølund B, Liljefors T, Krogsgaard-Larsen P (2005) Neuronal nicotinic acetylcholine receptors: structural revelations, target identifications, and therapeutic inspirations. J Med Chem 48:4705–4745

Kaas Q, Westermann JC, Craik DJ (2010) Conopeptide characterization and classifications: an analysis using ConoServer. Toxicon 55:1491–1509

Kaas Q, Westermann JC, Halai R, Wang CK, Craik DJ (2008) Conoserver, a database for conopeptide sequences and structures. Bioinformatics 24:445–446

Kang TS, Vivekanandan S, Jois SDS, Kini RM (2005) Effect of C-terminal amidation on folding and disulfide-pairing of α-conotoxin ImI. Angew Chem Int Ed 117:6491–6495

Koradi R, Billeter M, Wüthrich K (1996) MOLMOL: a program for display and analysis of macromolecular structures. J Mol Graph 14(51–55):29–32

Lopez-Vera1 E, Aguilar MB, Schiavon E, Marinzi C, Ortiz E, Cassulini RR, Batista CVF, Possani LD, de la Cotera EPH, Peri F, Becerril B, Wanke E (2007) Novel α-conotoxins from conus

spurius and theα-conotoxin EI share high-affinity potentiation and low-affinity inhibition of nicotinic acetylcholine receptors. FEBS J 274:3972–3985

Luo SL, Akondi KB, Zhangsun D, Wu Y, Zhu XP, Hu YY, Christensen S, Dowell C, Daly NL, Craik DJ, Wang CA, Lewis RJ, Alewood PF, McIntosh JM (2010) A typical α-conotoxin ltIA from conus litteratus targets a novel microsite of the $\alpha 3\beta 2$ nicotinic receptor. J Biol Chem 285:12355–12366

Luo SL, Nguyen TA, Cartier GE, Olivera BM, Yoshikami D, McIntosh JM (1999) Single-residue alteration in alpha-conotoxin PnIA switches its nAChR subtype selectivity. Biochemistry 38:14542–14548

Loughnan ML, Nicke A, Jones A, Adams DJ, Alewood PF, Lewis RJ (2004) Chemical and functional identification and characterization of novel sulfated α-conotoxins from the cone snail *Conus anemone*. J Med Chem 47:1234–1241

McIntosh JM, Corpuz GO, Layer RT, Garrett JE, Wagstaff JD, Bulaj G, Vyazovkina A, Yoshikami D, Cruz LJ, Olivera BM (2000) Isolation and characterization of a novel Conus peptide with apparent antinociceptive activity. J Biol Chem 275:32391–32397

McIntosh JM, Cruz LJ, Hunkapiller MW, Gray WR, Olivera BM (1982) Isolation and structure of a peptide toxin from the marine snail Conusmagus. Arch Biochem Biophys 5:280–292

McIntosh JM, Yoshikami D, Mahe E, Nielsen DB, Rivier JE, Gray WR, Olivera BM (1994) A nicotinic acetylcholine receptor ligand of unique specificity, alpha- conotoxin ImI. J Biol Chem 269:16733–16739

Millard EL, Daly NL, Craik DJ (2004) Structure-activity relationships and α-conotoxins targeting neuronal nicotinic acetylcholine receptors. Eur J Biochem 271:2320–2326

Möller C, Rahmankhah S, Lauer-Fields J, Bubis J, Fields GB, Marí F (2005) A novel conotoxin framework with a helix loop helix (Cs α/α) fold. Biochemistry 44:15986–15996

Nicke A, Loughnan ML, Millard EL, Alewood PF, Adams DJ, Daly NL, Craik DJ, Lewis RJ (2003) Isolation, structure, and activity of GID, a novel α4/7-conotoxin with an extended N-terminal sequence. J Biol Chem 278:3137–3144

Olivera BM, Cruz LJ (2001) Conotoxins, inretrospect. Toxicon 39:7–14

Olivera BM, Gray WR, Zeikus R, McIntosh JM, Varga J, Rivier J, de Santos V, Cruz LJ (1985) Peptide neurotoxins from fish-hunting cone snails. Science 230:1338–1343

Oliveral BM, Quik M, Vincler M, Mclntosh JM (2008) Subtype-selective conopeptides targeted to nicotinic receptors: concerted discovery and biomedical applications. Channels 2:143–152

Pahlke D, Freund C, Leitner D, Labudde D (2005) Statistically significant dependence of the Xaa-Pro peptide bond conformation on secondary structure and amino acid sequence. BMC Struct Biol 5:8

Park KH, Suk JE, Jacobsen R, Gray WR, McIntosh JM, Han KH (2001) Solution conformation of α-conotoxin EI, a neuromuscular toxin specific for the $\alpha 1/\delta$ subunit interface of *Torpedo* nicotinic acetylcholine receptor. J Biol Chem 276:49028–49033

Peng C, Tang SJ, Pi CH, Liu JL, Wang F, Wang L, Zhou WL, Xu AL (2006) Discovery of a novel class of conotoxin from Conus litteratus, Lt14a, with a unique cysteine pattern. Peptides 27:2174–2181

Peng C, Ye MY, Wang YF, Shao XX, Yuan DD, Liu J, Hawrot E, Wang CG, Chi CW (2010) A new subfamily of conotoxins belonging to the A-superfamily. Peptides 31:2009–2016

Pi CH, Liu JL, Peng C, Liu Y, Jiang XH, Zhao Y, Tang SJ, Wang L, Dong ML, Chen SW, Xu AL (2006) Diversity and evolution of conotoxins based on gene expression profiling of *Conus litteratus*. Genomics 88:809–819

Sun DD, Ren ZH, Zeng XY, You YW, Pan WG, Zhou MJ, Wang L, Xu AL (2010) Structure–function relationship of conotoxin Lt14a, a potential analgesic with low cytotoxicity. Peptides 32:300–305

Terlau H, Olivera BM (2004) Conus venoms: a rich source of novel ion channel targeted peptides. Physiol Rev 84:41–68

Weiss MS, Jabs A, Hilgenfeld R (1998) Peptide bonds revisited. Nat Struct Biol 5:676

Wuthrich K (1986) NMR of proteins and nucleic acids. Wiley, New York